

The Role of Millimeter VLBI Observations in AGN Research

T.P. Krichbaum, A. Witzel, and J.A. Zensus

Max-Planck-Institut für Radioastronomie, Auf dem Hügel 69, D-53121 Bonn, Germany

Abstract. VLBI at millimeter wavelengths (mm-VLBI) allows the detailed imaging of compact galactic and extragalactic radio sources with micro-arcsecond scale resolution, inaccessible by other observing techniques. Here we discuss the scientific potential of mm-VLBI for present and future research on ‘Active Galactic Nuclei’ (AGN) and their powerful relativistic jets. With the new generation of large radio telescopes and interferometer arrays operating in the millimeter radio bands (e.g. ALMA), the ultimate vicinity of super massive Black Holes, and eventually even their event horizon, could be imaged. With its large collecting area, and in combination with these future telescopes, the Sardinia Radio Telescope could form the World’s ‘sharpest’ astronomical imaging machine.

1. Introduction

Even after more than 40 years after Marten Schmidt’s discovery of the cosmological redshift of the hydrogen lines in 3C 273, and of astrophysical research on Active Galactic Nuclei (AGN) in general, the enigma of the origin of their extreme luminosity (ranging from radio to Gamma-ray bands) and the creation mechanism for the highly relativistic plasma jets (often extending over many hundred kpc) still is not solved. Although the majority of the scientific community regards accretion onto supermassive black holes as the most plausible explanation for the ‘quasar phenomenon’, many details of the astrophysical processes taking place in the centers of these most luminous objects in the Universe still remain unexplained. In particular is the question of how the relativistic jets are made, accelerated and confined not satisfyingly answered. In order to test existing theories (e.g. the Blandford-Payne magnetic slingshot mechanism), which try to explain the accretion process and the subsequent energy release and jet creation, the direct imaging of the innermost regions of Active Galactic Nuclei is of great importance. The technique of interferometry is the only observing method, which leads to such direct images.

In **Very Long Baseline Interferometry** (VLBI) the angular resolution can be improved, either by increasing the distance between the radio telescopes or by observing at shorter wavelengths. The first approach leads to VLBI with orbiting radio antennas in space (eg. VSOP, Hirabayashi et al. 2000), which however at present gives only an angular resolution of 0.2–0.3 mas ($1 \text{ mas} = 10^{-3} \text{ arcsec}$) at 5 GHz. The second possibility leads to VLBI at millimeter wavelengths (mm-VLBI), which furthermore facilitates the imaging of compact structures, which are self-absorbed (opaque), and therefore not directly observable, at the longer centimeter wavelengths. Nowadays, mm-VLBI observations are regularly performed at 86 GHz ($\lambda = 3.5 \text{ mm}$), where images with an angular resolutions of up to $\sim 50 \mu\text{as}$ ($1 \mu\text{as} = 10^{-6} \text{ arcsec}$) are obtained. The two upper parts of Table 1 summarize the stations, which participate in such global 3 mm-VLBI experiments. VLBI observations at even shorter wavelengths are technically possible (see e.g. Krichbaum et al. 1997 for VLBI at 215 GHz; Greve et al. 2002 for VLBI at 147 GHz), but have not yet passed the stage of test experiments on more than on single baselines. With the coming new generation of large millimeter telescopes and arrays (see Table 1, lower section), global VLBI observations at 2 and 1 mm wavelength should become possible within the next few years. Such observations would result in images of up to $\sim 20 \mu\text{as}$ resolution, which in the case of the quasar 3C 273 would correspond to a spatial resolution of ~ 400 Schwarzschild radii (for a $10^9 M_\odot$ black hole). One can therefore imagine that for less distant objects (e.g. for nearby radio-galaxies like M 87, Cyg A and 3C 84, or for the compact radio source Sgr A* in the Galactic Center), future ground based 1 mm-VLBI or space based 3 mm-VLBI should allow the direct imaging of the vicinity of supermassive black holes and eventually even the event horizon¹. Thus direct observational tests of general relativity and space-time curvature near large masses will become possible.

In addition to the basic motivation of trying to image the close vicinity of a black hole in an AGN with mm-VLBI, other questions related to the observed source activity (flux density variability, jet kinematics, broad band spectrum) are of direct interest. In jets of compact radio sources, mm-VLBI can detect structural changes at a relatively high observing frequency and in a very early evolutionary stage. This can be used to study the relation between flux density outbursts (broad band, from radio to Gamma-rays) and ejection of new jet components. Such ‘outburst-ejection’ correlations seem to be present in many blazars and are a direct signpost of the acceleration mechanism acting at the center. Through its very high angular resolution, mm-VLBI images of radio-jets also allow to locate moving features in the jet with very high accuracy. Jets of nearby ($z \leq 0.2$) galaxies can also be resolved transversely. All this

¹For Sgr A* the present upper limit to the source size is ~ 20 Schwarzschild radii (cf. Krichbaum et al. 1998).

facilitates a more precise determination of the structural variations and the jet kinematics. Images obtained from mm-VLBI furthermore allow to trace the jet curvature, frequently observed in many AGN, much closer to the nucleus. Such curvature, which increases towards the center, is an indicator of complicated internal plasma physics (e.g. hydrodynamic or magneto-hydrodynamic instabilities, oblique shocks) and possibly of twisted magnetic fields anchored in a rotating accretion disk.

2. The inner jet of 3C 273, a well studied case

In the following paragraph, we present some results for the inner jet of the quasar 3C 273, which can serve in this context as a typical example to illustrate the capabilities of mm-VLBI for future AGN research not only in this but also in other objects:

At sub-milliarcsecond resolution, 3C 273 shows a one sided core-jet structure of several milliarcseconds length. The jet breaks up into multiple VLBI components, which – when represented by Gaussian components – seem to separate at apparent superluminal speeds from the stationary assumed VLBI core. The cross-identification of the model-fit components, seen at different times and epochs, is facilitated by small (< 0.2 mas), and to first order negligible, opacity shifts of the component positions relative to the VLBI-core. Quasi-simultaneous data sets (cf. Fig. 1) demonstrate convincingly the reliability of the component identification, which results in a kinematic scenario, in which all detected jet components (C6 – C18) move steadily (without ‘jumps’ in position) away from the core (Fig. 4). For the components with enough data points at small (< 2 mas) and large (> 2 mas) core separations, quadratic fits to the radial motion $r(t)$ (but also for $x(t)$ –right ascension, and $y(t)$ –declination) represent the observations much better than linear fits. Thus the components seem to accelerate as they move out. The velocities range typically from $\beta_{app} = 3 - 8$ (for $H_0 = 100 \text{ km s}^{-1} \text{ Mpc}^{-1}$, $q_0 = 0.5$).

Dual-frequency maps obtained in 1995 (22/86 GHz) and 1997 (15/86 GHz) allow to measure the spectral index gradient along the jet (see Fig. 2). The spectrum of the jet oscillates between $-1.0 \leq \alpha \leq +0.5$ ($S_\nu \propto \nu^\alpha$). Most noteworthy, the spectral gradients did not change by much over the 2 year time interval, although different jet components occupied this region during this period. Therefore, the geometrical (eg. relativistic aberration) and/or the physical environment (pressure, density, B-field) in the jet must determine the observed properties of the VLBI components. Hence, we conclude that the latter do not form ‘physical entities’, but seem to react to the physical conditions in the jet fluid and from its boundaries.

Further evidence for a fluid dynamical interpretation comes from a study of the shape of the mean jet axis and the transverse width of the jet. Both oscillate

Station	D [m]	T_{sys} [K]	Gain [K/Jy]	η_A	SEFD [Jy]
Effelsberg, Germany	100	150	0.14	0.08	1070
Haystack, MA, USA	37	150	0.058	0.15	2590
Pico Veleta, Spain	30	120	0.14	0.55	860
VLBA (7), USA	25	150	0.032	0.18	4680
Onsala, Sweden	20	250	0.045	0.40	5550
Sest, Chile	15	200	0.038	0.60	5260
Metsähovi, Finland	14	300	0.017	0.30	17650
Nobeyama, Japan	45	150	0.17	0.30	880
Ovro, CA, USA	6x10.4	200	0.084	0.50	2380
Hat Creek, CA, USA	9x6.1	200	0.050	0.55	4000
Quabbin, MA, USA	14	300	0.026	0.47	11540
KittPeak, AZ, USA	12	150	0.026	0.64	5770
ALMA, Chile	64x12	100	1.82	0.70	55
GBT, WV, USA	110	100	1.00	0.35	100
CARMA, CA, USA	6x10+9x6	100	0.14	0.55	710
P. de Bure, France	6x15	100	0.18	0.51	560
SRT, Sardinia	64	100	0.35	0.30	290
LMT, Mexico	50	100	0.43	0.60	230
Yebes, Spain	40	100	0.13	0.30	770

Table 1. VLBI telescopes operating in the 3 mm band (86-100 GHz). The columns list the station name and location (col. 1), the antenna diameter (col. 2), a typical system temperature (col. 3), the antenna gain and aperture efficiency (col. 4 and 5) and the system equivalent flux density SEFD (col. 6). Antennas which regularly participate in global 3mm-VLBI campaigns are listed on top. The second part of the Table summarizes telescopes, which either participated in the past in such experiments, or which participate occasionally. The lower part of the Table lists some antennas (planned or under construction), which could participate in mm-VLBI in the future. For these antennas, the aperture efficiencies and the gains were roughly estimated based on data available in the internet and the literature. The detection sensitivity on a VLBI baseline between two antennas can be estimated by $\sigma_{[Jy]} = \eta^{-1} \cdot \sqrt{\text{SEFD}_i \cdot \text{SEFD}_j / (2Bt)}$, where B is the observing bandwidth in [Hz], t is the integration time in [sec], η is the correlation loss factor (0.88 for 2 bit sampling) and the SEFDs are taken from column 6 for two antennas i and j .

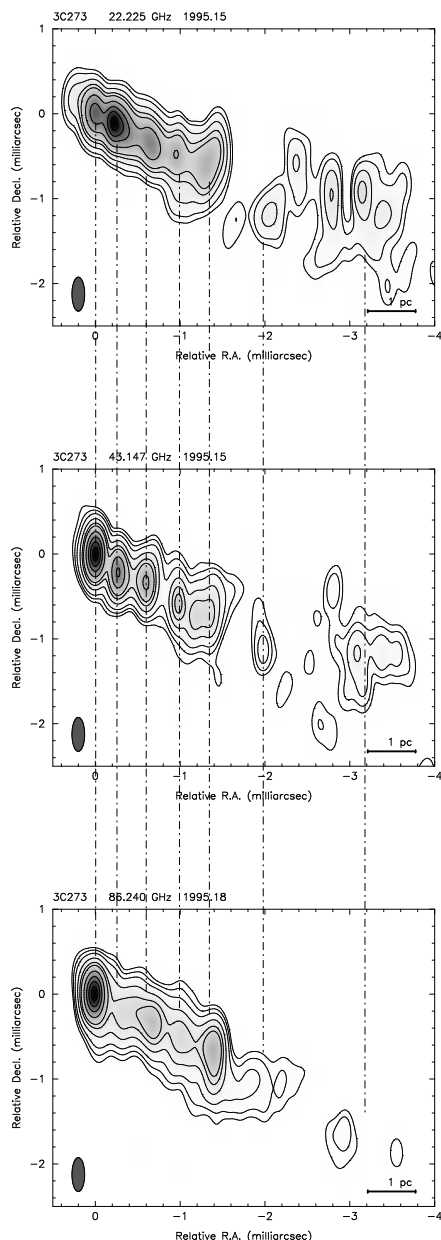


Fig. 1: 3C 273 at 22 GHz (top), 43 GHz (center), and 86 GHz (bottom) observed in 1995.15 – 1995.18. Contour levels are -0.5, 0.5, 1, 2, 5, 10, 15, 30, 50, 70, and 90 % of the peak of 3.0 (top), 5.4 (center), and 4.7 Jy/beam (bottom). For the 22 GHz map, the 0.5 % contour is omitted. The restoring beam is 0.4×0.15 mas in size, oriented at $pa = 0^\circ$. The maps are centered on the eastern component (the core), the dashed lines guide the eye and help to identify corresponding jet components.

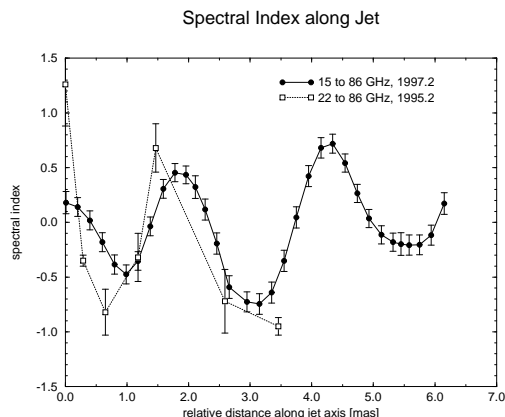


Fig. 2: Spectral index variations along the jet. For 1997 (circles, solid lines), the spectral index gradient is calculated directly from the intensity profiles of the maps at 15 and 86 GHz. For 1995 (squares, dashed line), the spectral indices were derived from Gaussian component model fits at 22 and 86 GHz. We note that during 1995 – 1997, different jet components occupied this jet region. The spectral profile along the jet, however, did not change very much.

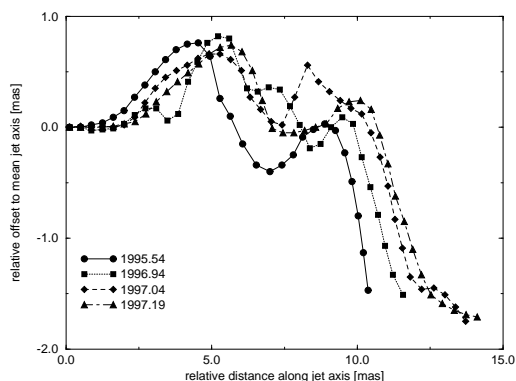


Fig. 3: The motion of the mean jet axis in the inner jet of 3C 273 at 15 GHz. Symbols denote for different epochs: 1995.54 (circles), 1996.94 (squares), 1997.04 (diamonds), and 1997.19 (triangles). The transverse oscillations of the ridge line are measured relative to a straight line oriented along $pa = 240^\circ$. We note the systematic longitudinal displacement of maxima and minima. This corresponds to an apparent pattern velocity of $\beta_{app} \simeq 4.2$, which is by a factor of up to 2 slower than the component motion.

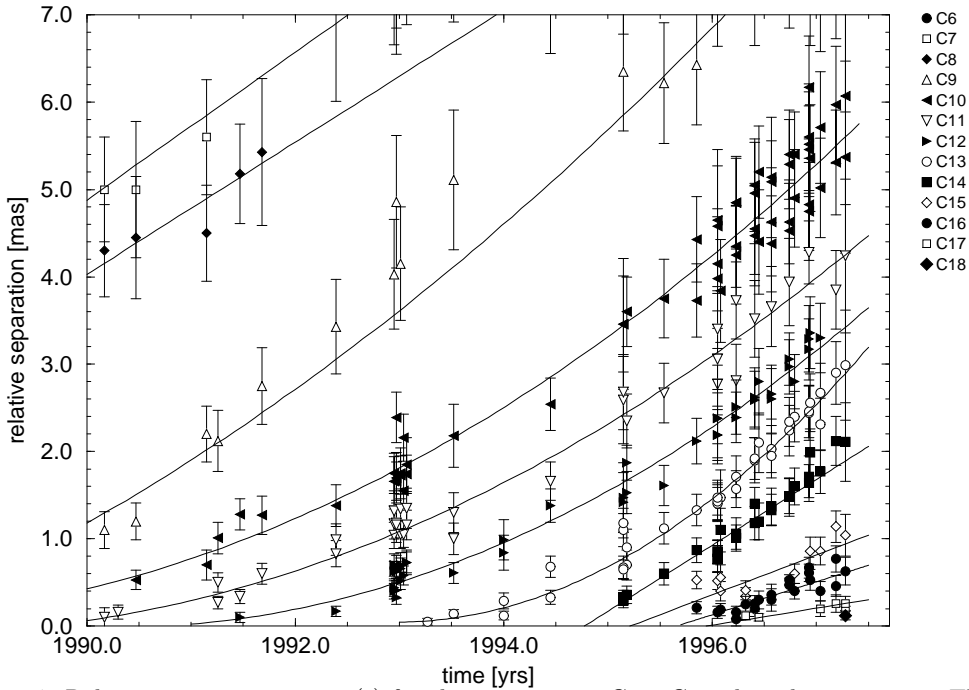


Fig. 4: Relative core separations $r(t)$ for the components C6 – C18 plotted versus time. The legend on the right identifies symbols with VLBI components. The lines are least square fits to the data. Note the acceleration of the motion. For the inner and newest jet components ($r < 1$ mas, $t > 1996$) the data do not yet allow to discriminate between constant and accelerated motion.

quasi-sinusoidally on mas-scales. At 15 GHz, the variation of the ridge-line with time could be determined from 4 VLBA maps obtained during 1995 – 1997 (Fig. 3). The maxima and minima of the ridge-line are systematically displaced. This ‘longitudinal’ shift suggests motion with a pattern velocity of $\beta_{app} = 4.2$, about a factor of 2 slower than the maximum observed jet speed ($\beta_{app} \leq 8$). The sinusoidal curvature of the jet axis, however, could also indicate jet rotation rather than longitudinal waves. Helical Kelvin-Helmholtz instabilities propagating in the jet sheath (cf. Lobanov & Zensus 2001) could mimic such rotation, which, when seen in projection, would also explain the spectral index oscillation seen in Figure 2.

Additional support for a rotation of the jet around its axis comes from the study of the ejection of new jet components, appearing shortly after prominent flux density outbursts. From Figure 4 and from the VLBI maps, we determined the velocity and the direction of ejection of such new jet components, by fitting a straight line to the inner region of the jet (for $r \leq 0.5$ mas). From these fits we also obtained the time of ejection, which correlates remarkably well with the occurrence of the known millimeter/optical outbursts. In Figure 5 we plot the ejection velocity and its direction (position angle) versus the time of ejection (t_0). It is remarkable that ejection velocity and ejection direction show systematic, quasi-periodic variations, indicating a precession of the footpoint of the jet with

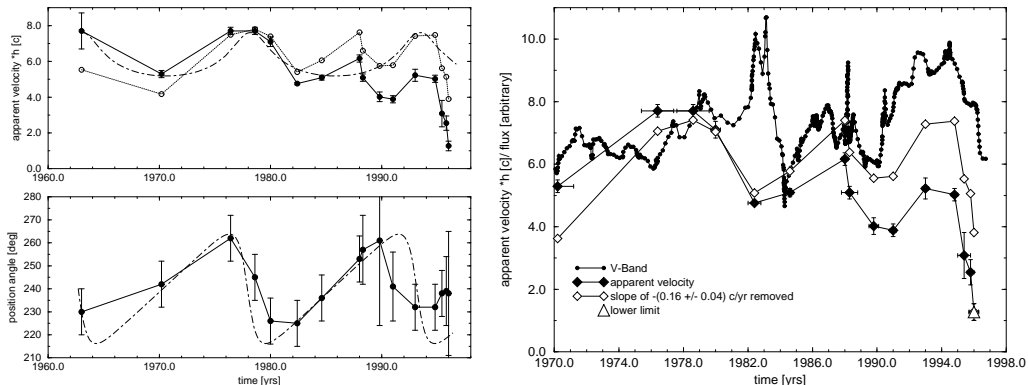


Fig. 5: Left: Apparent velocity β_{app} (top) and position angle (bottom) of new ejected jet components plotted versus time of ejection t_0 . On top, open circles show the velocity after removal of an overall slope of $d\beta_{app}/dt = -(0.16 \pm 0.04) \text{ yr}^{-1}$. Superimposed in both figures as a dashed line is a simple precessing beam model (cf. Abraham & Romero, 1999). Whereas the position angle follows the model, the apparent velocity shows an additional maximum near 1988. The data indicate a rotation or precession of the jet base with a period of 15–16 yrs. Right: Apparent velocity β_{app} of the jet components plotted versus time of ejection t_0 (filled diamonds). Again, open diamonds show β_{app} after removal of the afore mentioned slope. Superimposed to the velocity is the optical V-Band light-curve (from Türler et al. 1999). The flux density at V-Band is in arbitrary flux units. In 1982 – 1997 a correlation between optical flux and ejection velocity is indicated.

a period of 15–16 yrs (see also: Abraham & Romero, 1999). In 1982 – 1997 a correlation between optical flux and ejection velocity is indicated (Fig. 5, right panel). At earlier times such a correlation is less obvious, however can not be excluded, since at these times the accurate determination of the ejection velocity was limited by the quality and time sampling of the early (pre 1990) VLBI data. Qian et al. (2001) explain the correlation of ejection velocity and optical flux by a periodic modulation of the jet flow Lorentz factor in a binary black hole system with a precessing accretion disk.

For many AGN, a correlation between flux density variability and ejection of VLBI components is suggested. In 3C 273 we identified 13 jet components (C6 – C18) and traced their motion back to their ejection from the VLBI core. The typical measurement uncertainty for the ejection times t_0 ranges between 0.2 – 0.5 yr. In Figure 6 (left) we plot t_0 and the flux density variability at 22 – 230 GHz. We also add the Gamma-ray detections of 3C 273 from EGRET. In Figure 6 (right) we plot the onset times of the mm-flares derived from these light curves (Türler et al. 1999) together with the VLBI ejection time (t_0) and the Gamma-ray fluxes. For each onset of a mm-flare, we find that a new jet component was ejected.

Although the time sampling of the Gamma-ray data is quite coarse, a relation between component ejection and high Gamma-ray flux appears very likely (note that each Gamma-detection already means higher than usual γ -

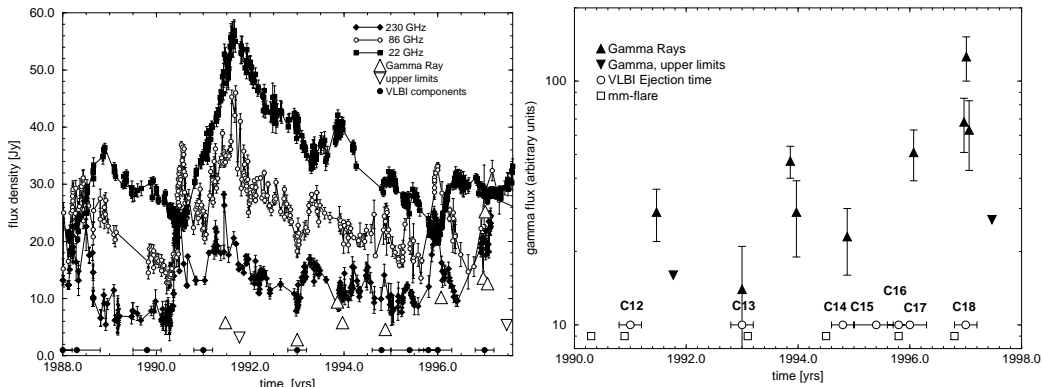


Fig. 6: Left: Flux density variations at 230 GHz (filled diamonds), 86 GHz (open circles) and 22 GHz (filled squares). Upward oriented triangles denote Gamma-ray fluxes from EGRET, downward oriented triangles are upper limits. The extrapolated ejection times of the VLBI components and their uncertainties are indicated by filled circles with horizontal bars along the time axis. Right: Broad-band flux density activity and component ejection. VLBI component ejection (open circles), Gamma-ray fluxes (triangles, downward oriented for upper limits) and onset-times for the millimeter flares (open squares, from Türler et al. 1999) are shown versus time. Labels denote the component identification from VLBI.

brightness). From a more detailed analysis (Krichbaum et al. 2002) we obtain for the time lag between component ejection and onset of a mm-flare: $t_0 - t_0^{\text{mm}} = 0.1 \pm 0.2 \text{ yr}$. If we assume that the observed peaks in the Gamma-ray light-curve are located near the times t_0^γ of flux density maxima, we obtain $t_0^\gamma - t_0^{\text{mm}} = 0.3 \pm 0.3 \text{ yr}$. Although the Gamma-ray variability may be faster, this result is fully consistent with the more general finding of enhanced Gamma-ray fluxes mainly during the rising phase of millimeter flares. We therefore suggest the following tentative sequence of events: $t_0^{\text{mm}} \leq t_0 \leq t_0^\gamma$ – the onset of a millimeter flare is followed by the ejection of a new VLBI component and, either simultaneously or slightly time-delayed, an increase of the Gamma-ray flux. If we focus only on those VLBI components, which were ejected close to the main maxima of the Gamma-ray light-curve in Figure 6, we obtain time lags of $t_0^\gamma - t_0$ of $\leq 0.5 \text{ yr}$ for C12, $\leq 0.9 \text{ yr}$ for C13, $\leq 0.2 \text{ yr}$ for C16 and $\leq 0.1 \text{ yr}$ for C18. In all cases, the Gamma-rays seem to peak a little later than the time of component ejection. With $\beta_{\text{app}} \simeq 4$ near the core, the Gamma-rays would then escape at a radius $r_\gamma \leq 0.1 \text{ mas}$. This corresponds to $r_\gamma \leq 2000$ Schwarzschild radii (for a $10^9 M_\odot$ black hole) or $\leq 6 \cdot 10^{17} \text{ cm}$, consistent with theoretical expectations, in which Gamma-rays escape the horizon of photon-photon pair production at separations of a few hundred to a few thousand Schwarzschild radii.

3. The Contribution of the SRT

To date, VLBI at 3 mm and shorter wavelengths is still limited in sensitivity. Presently, a few dozens of compact objects with typical flux densities

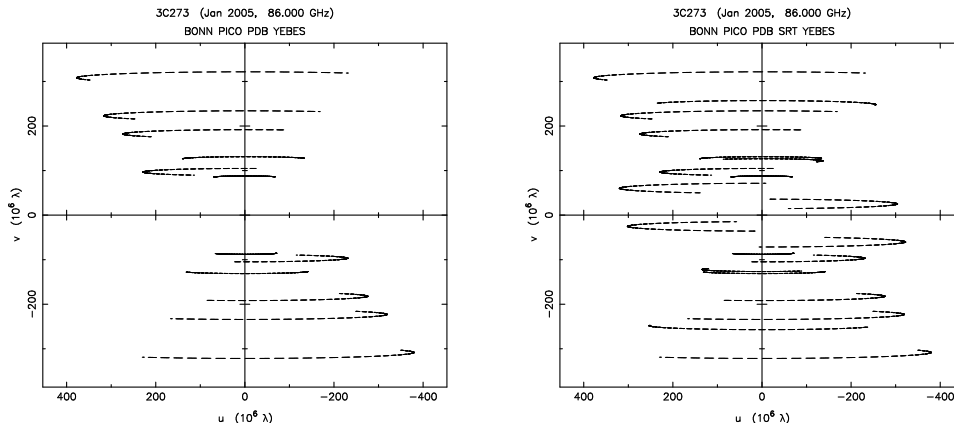


Fig. 7: A simulation of a future uv-coverage for 3C 273 with the largest millimeter antennas in Europe. On the left the uv-coverage is shown for Bonn, Pico Veleta, Plateau de Bure (PDB) and Yebes. On the right the Sardinia Radio Telescope (SRT) is added.

$S_{86\text{GHz}} \geq 0.5 - 1 \text{ Jy}$ can be reliably imaged (e.g. Lobanov et al. 2000). This limitation can be overcome by (i) adding more collecting area, (ii) by enlarging the observing bandwidth and data recording rate (presently $\leq 256 \text{ Mbits/sec}$ and $\leq 128 \text{ MHz}$), and (iii) by correcting phase fluctuations introduced by the atmosphere (water vapor radiometry, dual frequency VLBI). Another limitation is the non-uniformity of the uv-coverage, in particular the lack of short interferometer baselines in present 3 mm-VLBI. Since many AGN are partially resolved and show relatively long VLBI jets even at millimeter wavelengths (at 86 GHz AGN jets can extend over more than 200 beam sizes, cf. Krichbaum et al. 1999), the addition of large and sensitive millimeter telescopes at moderate separations from the existing telescopes is of considerable importance for reliable images. In this context and not only because of its large collecting area, but also due to its southern location within Europe, could the Sardinia Radio Telescope (SRT) make a significant contribution to the scientific research of compact galactic and extragalactic radio sources at millimeter wavelengths.

At 86 GHz, the detection threshold on a single VLBI baseline (7σ , 256 Mbits/sec, 60 sec integration time) is at present 50–100 mJy on the most sensitive baselines (eg. Pico Veleta to Effelsberg) and 300–400 mJy on VLBA baselines. With the telescopes summarized in the top section of Table 1, the baseline sensitivities within Europe are presently a factor of 2–3 higher than in America. This will change when the Green Bank Telescope (GBT) and the Mexican Large Millimeter Telescope (LMT) start observing at 3 mm. In the near future, also the phased IRAM interferometer on Plateau de Bure (six 15 m antennas) and the 40 m antenna in Yebes could participate in mm-VLBI. This should lower the detection threshold for mm-VLBI in Europe to 30–40 mJy (at 86 GHz). The combination of Plateau de Bure, Yebes and the SRT with the other existing millimeter antennas (Table 1), will not only improve this sensitivity by another

factor of 1.5–2. Equally important, this will also ameliorate the uv-coverage on short uv-spacings (see Fig. 7), in particular for sources which are near or below the celestial equator, and which will be the prime targets for global mm-VLBI with ALMA. With ALMA, the single baseline sensitivity between ALMA, the SRT and other large millimeter telescopes will be as low 5 – 10 mJy. Under the assumption of future enhanced bandwidth and Giga-bit recording and with full atmospheric phase correction applied, it could even reach the sub-milli Jansky level. So future mm-VLBI could reach the same sensitivity and could observe the same number of compact sources as cm-VLBI does nowadays.

Acknowledgments. Many of the results shown here originate from millimeter-VLBI observations with the following observatories: Effelsberg (MPIfR), Onsala and Sest (OSO), Pico Veleta (IRAM), Haystack (MIT-NERO), Hat Creek (BIMA), Owens Valley (OVRO), and the VLBA (NRAO). We like to thank all the people who contributed to these observations for their efforts and for their continuing enthusiasm to push VLBI to higher frequencies. TPK also likes to thank the organizers of the SRT-conference for their support and hospitality.

References

- [1] Abraham Z., & Romero G.E., 1999, *A&A* *344*, 61.
- [2] Greve A., et al., ‘147 GHz VLBI observations with Pico Veleta and Metsähovi’, 2002, *A&A*, submitted.
- [3] Hirabayashi H. et al., 2000, *PASJ* *52*, 955.
- [4] Krichbaum T.P., et al., 1997, *A&A* *323*, 17.
- [5] Krichbaum T.P., et al., 1998, *A&A* *335*, L106.
- [6] Krichbaum T.P., et al., 1999, in: Second Millimeter-VLBI Science Workshop, eds. A. Greve & T.P. Krichbaum, IRAM Grenoble, p.5.
- [7] Krichbaum T.P., et al., ‘High Frequency VLBI Observations of 3C 273’, 2002, *A&A*, submitted.
- [8] Lobanov A., Krichbaum T.P., Graham D.A., et al., 2000, *A&A* *364*, 391.
- [9] Lobanov A., & Zensus J.A., 2001, *Sci* *294*, 128.
- [10] Qian S.J., Zhang X.Z., Krichbaum T.P., et al., 2001, *ChJAA* *1*, 236.
- [11] Türler M., Courvoisier T.J.-L., & Paltani S., 1999, *A&A* *349*, 45.